Nonlinear Stochastic Differential Equations Modeling and Analysis of Multi-Stage Manufacturing Systems Dynamics

Satish T.S. Bukkapatnam, Hui Yang, Utkarsh Mittal, and Leandro G. Barajas

Abstract— **Modern manufacturing enterprises have invested in a variety of sensors and IT infrastructure to increase plant floor information visibility. This offers an unprecedented opportunity to track performances of manufacturing systems from a dynamic, as opposed to static, sense. Conventional static models are inadequate to model manufacturing system performance variations in real-time from these large non-stationary data sources. This paper addresses a physics-based approach to model the performance outputs (e.g., throughputs, uptimes, and yield rates) from a multi-stage manufacturing system. Unlike previous methods, interactions between degradation and repair dynamics that influence downtime distributions in such manufacturing systems are explicitly considered. Regardless of the level of automation in an operation (human or fully mechanized), the process over time undergoes degradation of the state (condition) due to component level mechanized or electrical degradations (wear, or human fatigue/propensity to errors). The repair efforts aimed at restoring the states. Sigmoid function theory is used to remove discontinuities in the models. The resulting model is validated using real-world datasets acquired from the General Motor's assembly lines, and it is found to capture dynamics of downtime better than traditional exponential distribution based simulation models.**

Index Terms— **nonlinear stochastic differential equation (n-SDE) model, mean time between failure (MTBF), mean time to repair (MTTR), recurrence analysis, multi-stage manufacturing systems**

I. Introduction

Increasing global competition is forcing many automotive, aerospace and microelectronic manufacturing systems towards low margins and lean operations. More than ever, customers are demanding lower prices, short turnaround times, higher quality, and customized designs. In order to stay competitive under volatile demands as well as internal and external disruptions, modern manufacturing systems need to dynamically adjust product mix, plan near-term capacity, and manage suppliers and dealers with little time latency.

Accurate real-time prediction of performance is essential for making a manufacturing system respond in a fast and flexible manner to demand variations and disruptions. Performance of manufacturing systems, such as automotive manufacturing lines, are typically expressed in terms of throughput rates, throughput losses due to breakdowns, blocking and starving, and WIP levels [1].

However, conventional static models are inadequate for predicting these performance variables in real-time, therefore, dynamic models are necessary. Modern manufacturing systems are pervasively networked to carefully monitor and record most events and statuses, e.g., start and end of operations, fault events, exceptions and errors, etc. Hundreds of messages related to performance variables can be generated in every second. Dynamic models can compactly capture information from these real-time data sources and thus help track the performances of a manufacturing system from a dynamic, as opposed to conventional static, sense.

Recent advancements on sensing techniques and computing power have compelled the research community to show a renewed interest in continuous flow modeling approaches [2-7]. Continuous flow modeling approaches can offer an effective balance between accuracy and speed. These approaches essentially model the parts movement in a manufacturing system as a fluid flow expressed in the form of differential equations. This is a reasonable assumption that enable us to capture dynamics of several manufacturing systems including automotive and semiconductor production lines where part inter-release time-scales are much shorter than those for other perturbation events. These models offer several advantages including faster simulations and enhanced identification of the system dynamic patterns compared to discrete-event simulations (DES). While queuing network models and micro DES have received significant attention, aggregate modeling has received little attention in the domain of manufacturing systems. Many of the recent pioneering

Manuscript received December 18, 2008. This work is supported in part by the National Science Foundation under grant CMMI-0729552 and in part by the General Motors.

Satish T.S. Bukkapatnam, Hui Yang and Utkarsh Mittal are with School of Industrial Engineering and Management, Oklahoma State University, Stillwater, OK 74075 USA (e-mail: satish.t.bukkapatnam@okstate.edu, hui.yang@okstate.edu, Utkarsh@okstate.edu).

Leandro Barajas is with the Manufacturing Systems Research Laboratory in General Motor R&D Center, Warren, MI, 48090 (e-mail: leandro.barajas@gm.com).

works have applied these models to gain certain crucial qualitative insights into the plant-floor and into the enterprise-level system characteristics [2-12]. Few works have shown the potential of time-aggregated flow models for performance monitoring and prediction.

We present an approach that uses the sigmoid function theory to relax certain assumptions made on the instantaneous nature of up and down time events. The resulting simulation model is found to capture the dynamics of downtime better than conventional exponential distribution based simulation models. The remainder of this paper is organized as follows: Section II presents a physics-based nonlinear stochastic differential equation (n-SDE) modeling approach; Section III demonstrates the n-SDE model parameterization using a genetic algorithm, comparisons of the resulting probability density functions (PDF) of the n-SDE and Exponential models versus the actual realizations, and nonlinear dynamic quantification of the investigated models versus the actual field data. Finally, Section IV presents the conclusions of the reported research and perspectives on future investigations.

II. Physics Based N-SDE Modeling Approach

Physics-based models use the first-principle physical and logical relationships in manufacturing systems to derive functional forms, and the aggregated line statistics to parameterize the models (just as how one derives DES models). For a simple N-stage manufacturing system, the change in the length of the buffer at the downstream of the k^{th} operation is given by

$$dL_k/dt = u_{k-1} - u_k \quad (1)$$

where u_k is the throughput velocity of operation k, L_k is the buffer inventory level. Typically, u_k is modeled using random processes μ_k and ν_k as

$$u_k = \mu_k - \nu_k \quad (2)$$

where μ_k is the processing rate during uptime, ν_k is the throughput rate loss due to downtime (alternative treatments of machine breakdown as a valve or a switch have been considered) , and $u_k = 0$ during downtime [13]. Downtime in many manufacturing system operations (see Fig. 1) can occur due to the following three reasons: (1) Machine breakdown and repair that takes place during times $t \in \mathbb{T}_{repair}$, (2) Starving (upstream buffer is empty) that takes place during times $t \in \mathbb{T}_{starve}$ and/or (3)Blocking (downstream buffer is full) that takes place during times $t \in \mathbb{T}_{block}$, i.e.,

$$u_k = 0 \text{ if } (L_k \le 0,\ L_{k+1} > L_{k+1}^{max},\ t \in \mathbb{T}_{repair}) \quad (3)$$

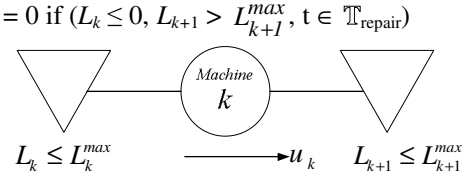

Fig. 1 Blocking and starving operation in an assembly line

The aforementioned flow modeling approaches have traditionally been used for qualitative analysis of system dynamics and not for real-time performance estimation. However, discontinuities in flow adversely affect the integration routines used to solve the model, and often cause the routines to become unstable. Sigmoid function theory is applied to derive equivalent analytic forms of the vector flow fields, whose integration methods pose less numerical instability issues and is expected to enable much faster simulation of system dynamics.

As shown in Fig. 2, the operation downtime due to machine breakdown and repair is simulated from a dynamic interplay between the machine degradation condition β and the restoration effort ρ. Intuitively, the machine will breakdown or, in general, operation down-state will set in if the machine condition drops below a threshold β^0. At this point the restoration process which proceeds from its base level ρ^- will start. As the restoration efforts (including diagnostics, disassembly and repair) proceed, the machine condition or operation state steadily bottoms out, improves from its lowest level β^- and above to a full restoration level β^+. About this point, the restoration efforts are relaxed out.

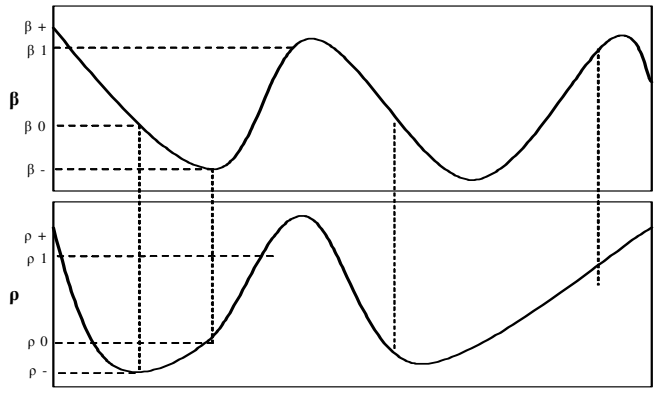

Fig. 2 Illustrative diagram of degradation and restoration variable dynamics

Such a dynamic interplay can be effectively captured using coupled nonlinear stochastic differential equations (n-SDEs) [5, 6]. For example, the machine degradation dynamics can be captured using a first order nonlinear differential equation of the form

$$\frac{d\beta}{dt} = K_1 \cdot \mathrm{sgm}\left(w_1(a_1 - \beta)\right)\mathrm{sgm}\left(-w_2(\rho - a_2)\right) + K_2 \cdot \mathrm{sgm}\left(w_3(\rho - a_3)\right)\mathrm{sgm}\left(w_4(\beta - a_4)\right) \quad (4)$$

Here, the first term captures the rate at which the operation (machine or operator state) degrades over time, and the second term determines the rate at which the system state responds to the restoration efforts. The restoration (damage-repair) dynamics is captured using the following second order differential equation

$$\frac{d^2\rho}{dt^2} = K_3 \cdot \mathrm{sgm}\left(w_5(\dot{\rho} - a_5)\right)\mathrm{sgm}\left(w_6(\beta - a_6)\right) + K_4 \cdot \mathrm{sgm}\left(w_7(a_7 - \beta)\right)\mathrm{sgm}\left(w_8(a_8 - \dot{\rho})\right) \quad (5)$$

where $a_{1\text{-}8}$ and $w_{1\text{-}8}$ are the threshold values and $K_{1\text{-}4}$ and the weights of sigmoid functions of the form

$$\mathrm{sgm}\left(w_j(\beta - a_j)\right) = \left(1 + e^{-w_j(\beta - a_j)}\right)^{-1} \quad (6)$$

which are the structural parameters of the model. Evidently, such sigmoid functions can be used to adjust throughput rate for each operation for downtime as well as for starve/block conditions as

$$u_k = \mu_k sgm(L_k)sgm(L_{k+1}^{max} - L_{k+1})sgm(\beta_k - \beta_k^0) \quad (7)$$

The parameters of sigmoid functions are chosen to meet the numerical stability and failure and repair time distributions of various operations. The functions in a way work like smooth switches between the up and down models of a machine. Such functional forms have been used to model, from experimental data, the fatigue fracture growth in metallic materials [14].

It is possible to adjust the distribution of some of the threshold parameters $a_{1\text{-}8}$ and $w_{1\text{-}8}$ to have the time-intervals between successive threshold crossings of follow an extremely skewed (e.g., exponential-like) marginal distributions and recurrence patterns (a nonlinear systems counterpart of the correlation structure) resembling those of the actual TTR and TBF. Towards this end, one needs to establish, preferably closed form, relationships between certain model parameters and the parameters that describe the distribution of TTR and TBF.

The model presented by Eq. (1), (4)-(6) and, consequently, TBF and TTR are deterministic. The approximate TBF is given by:

$$TBF \approx (a_1 - a_7)/K_1 + (a_1 - a_4)/K_2 \quad (8)$$

It is possible to adjust the distributions of a's and w's to have the time-intervals between successive threshold crossings of β to follow a skewed and multimodal distribution that mimics that of TBFs from actual line operations.

Observation: *A uniform perturbation of a_7 creates skewed and near-exponential distributions for TBF and TTR.*

The intuition here is that a symmetric perturbation of the threshold value a_7 creates a 50% chance that the threshold is lowered within the next time interval. This is equivalent to creating a short downtime event. By appropriate perturbation of threshold values it is possible to capture the heavily skewed (e.g., exponential) and multimodal downtime distributions.

However, parameterization of these models using historical fault realizations, such as historical records of time between failure (TBF) and time to repair (TTR), can be significantly challenging. We used a genetic algorithm for parameterization. The following fitness function *Op* defined in Eq. 8 is based on the empirical distributions of TTR and TBF obtained through histogram transformation of actual data and the model outputs:

$$Op = 100\left(\frac{\sum_{k=1}^{N_0}(HistTBF(k) - HistTBFa(k))^2}{N_0} + \frac{\sum_{k=1}^{N_1}(HistTTR(k) - HistTTRa(k))^2}{N_1}\right) + 10\left(\frac{\sum_{k=N_0+1}^{N_0+N_2}(HistTBF(k) - HistTBFa(k))^2}{N_2} + \frac{\sum_{k=N_1+1}^{N_1+N_3}(HistTTR(k) - HistTTRa(k))^2}{N_3}\right) + \left(\frac{\sum_{k=N_0+N_2+1}^{N_0+N_2+N_4}(HistTBF(k) - HistTBFa(k))^2}{N_4} + \frac{\sum_{k=N_1+N_3+1}^{N_1+N_3+N_5}(HistTTR(k) - HistTTRa(k))^2}{N_5}\right) \quad (9)$$

where k is the bin index. The histograms of TBF from the model (*HistTBF*) and the actual data (*HistTBFa*) are divided into three areas: N_0, N_2, N_4 are the number of bins used for the three areas to compare histogram transformations of TBF distribution from the model (*HistTBF*) with that from actual data (*HistTBFa*). Similarly, N_1, N_3, N_5 are the corresponding bins used to compare histogram transformations of TTR distribution from the model (*HistTTR*) with actual historic data (*HistTTRa*). The weights for the three areas of the histogram are assigned to be 100, 10, 1 that signify their relative importance from an operational standpoint. For instance, the values in the histogram bins with a weight of 100 are considered to be in the normal range of TBF/TTR, while the bins with smaller weights are taken to capture the highly infrequent instances of TBF/TTR where the number of samples is few. We parameterized the n-SDE models for each of the 18 machines in a real-world assembly line segment. The line segment considered for the present investigation consists of 18 stations of which 17 are allocated in tandem. One pair of stations is located in a parallel arrangement in the assembly line. We used the actual occurrences of various faults to derive distributions for TBF and TTR. The simulated as well as the actual TBF and TTR data were gathered over a two-month long period.

III. N-SDE Model Parameterization and Results

The Genetic Algorithm (GA) aims to determine the optimal values for 17 n-SDE model parameters namely a_1, a_2, a_3, a_4, a_5, a_6, a_{71}, a_{72}, a_8, k_{11}, k_{12}, k_{21}, k_{22}, k_{31}, k_{32}, k_{41}, k_{42} that reduce *Op* values to below 10^{-2}, such that TTR and TBF distributions closely match with those derived from the actual data. The GA procedure begins with the generation of the initial set of 50 different combinations of parameter vector values that are random within the allowable range for the 17 parameters n-SDE model. Each parameter was encoded as 35-bit long binary string. The objective function *Op* corresponding to this generated set of parameters is evaluated. Standard genetic operators like roulette-wheel selection, crossover, and mutation are used to generate a new set of 20 coded parameter values and the fitness function is then reevaluated. The GA terminates after the maximum number of iterations are reached or when the Genetic Algorithm converges.

TABLE 1. COMPARISON OF RESULTS BETWEEN GENETIC ALGORITHM AND OTHER NONLINEAR OPTIMIZATION METHODS

	Nelder simplex	GA	GA+ Nelder simplex	Actual
Op	4.86E-04	2.39e-005	2.36e-005	
MeanTTR	2	16.94	17.45	19.93
MeanTBF	20	71.74	72.46	78.64
StdTBF	38.03	126.17	128.44	147.42
StdTTR	3.34	39.93	51.71	66.20

For the cases examined, GA is found to converge in less than 50 iterations. To refine the fitness of the solutions a Nelder-Mead simplex method is used. Once the fitness improvement rate drops below a threshold level, it is assumed that the parameter values lie in the basin of the global minimum because non-gradient based stochastic GA optimization methods are known to locate the basin (trough/crest) of the global optimum with a very high probability. The results obtained by using GA, Nelder Simplex, and GA followed by simplex are compared in the Table 1, which show that minimum deviation is obtained by using First GA and then simplex, rather than GA alone.

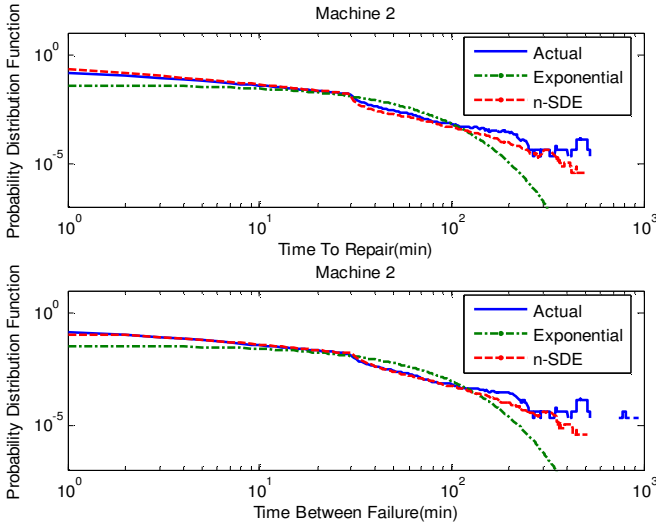

Fig. 3 *Comparison of marginal PDFs of TTR and TBF obtained from actual data (blue), n-SDE model (red) and exponential distribution model (green)*

The resulting GA-parameterized model can capture the dynamics of machine degradation as well as the distributions of downtime, especially the time between failures (TBF) and time to repair (TTR) better than conventional exponential distribution models. For instance, Fig.3 shows the marginal PDFs of TTR for an operation at a assembly station obtained from the actual historical data (solid blue line) vs. the distribution obtained from the model (red dash line) vs. the one obtained using the best fit exponential distribution (green dash dotted line).

TABLE 2. COMPARISON OF MEAN, STANDARD DEVIATION, % DEVIATION OF MEAN AND STANDARD DEVIATION FOR MACHINE 2 TTR AND TBF

Mean TTR		Std Dev TTR		Mean TBF		Std Dev TBF	
Actual	Model	Actual	Model	Actual	Model	Actual	Model
9.41	9.24	13.59	15.11	27.35	24.71	29.42	25.28
% dev.		% dev		% dev		% dev	
1.81		10.1%		9.67%		14.05%	

Table 2 compares the mean, standard deviation, % deviation between model for TTR and TBF for machine 2. Moreover, the investigated model shows a mean square error which is one order in magnitude smaller than the one from the exponential model.

Fig. 4 shows the variations of processing velocity with time for Machine 2. Maximum processing velocity for Machine 2 obtained from the actual data is 129 jobs/hour. This value is likely to occur, as is evident from Eq. (7), whenever the upstream buffer is full and the downstream buffer is empty and the machine is up. Also evident from the examining the histogram of the processing velocities (see Fig. 5) is that the machine is down for longer duration than when it is operating at the peak velocity.

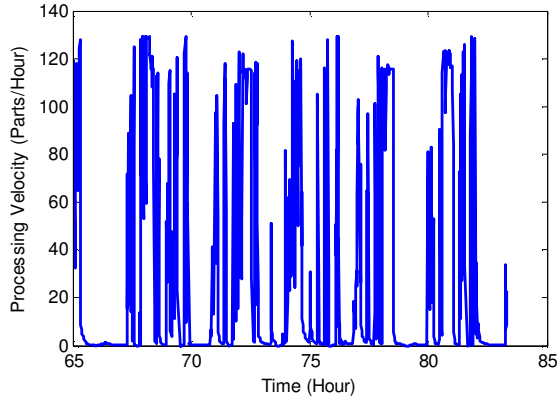

Fig. 4 *Processing Velocity for Machine 2*

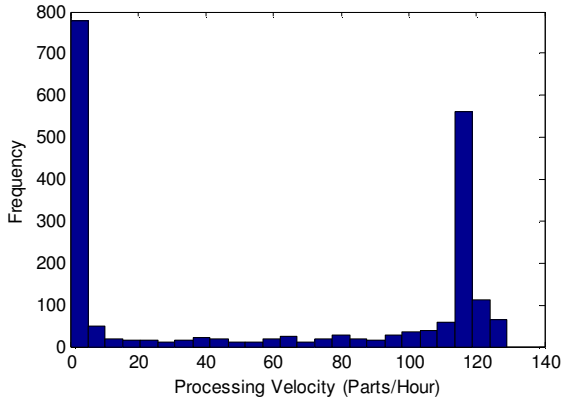

Fig. 5 *Histogram for Processing Velocity for Machine 2*

Table 3 shows the comparison between the processing velocity, expressed in terms of jobs per hour, from actual data versus the model. The average jobs/hour (processing velocity) from the actual and the model are 37.29 jobs/hour and 39.50 jobs/hour, respectively. The deviation between the model and the actual is 5.59%, which makes it quite comparable.

TABLE 3. COMPARISON OF PROCESSING VELOCITY BETWEEN MODEL AND ACTUAL

Jobs/Hour		%Deviation Jobs/Hour
Actual	Model	5.59 %
37.20	39.50	

Fig. 6 and Fig.7 compare the mean time to repair (MTTR) and mean time between failure (MTBF) for the 18 machines from the model vs. the actual data. The actual statistics are shown in brown bars and the model outputs are shown in blue. The comparisons show that the proposed model can capture the MTTR and MTBF variations from machine to machine for the investigated assembly line segment. The result shows that MTBF computed from the model lies within 3-10% of that computed from the actual data for 10 out of 18 machines. The model-computed MTBF values for the remaining 8 machines vary on an average by 24% relative to those computed from actual data. Similarly, the model-computed TTR values for 10 machines vary between 2-8% of those computed from the actual data, and vary by an average of 28% from those computed from the actual data for the remaining 8 machines.

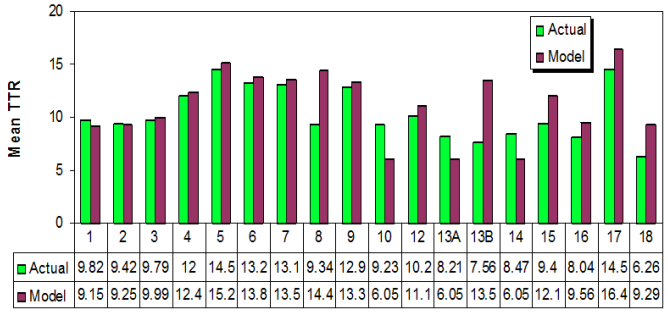

	1	2	3	4	5	6	7	8	9	10	12	13A	13B	14	15	16	17	18
Actual	9.82	9.42	9.79	12	14.5	13.2	13.1	9.34	12.9	9.23	10.2	8.21	7.56	8.47	9.4	8.04	14.5	6.26
Model	9.15	9.25	9.99	12.4	15.2	13.8	13.5	14.4	13.3	6.05	11.1	6.05	13.5	6.05	12.1	9.56	16.4	9.29

Fig. 6 *Comparison of Mean TTR (Model vs. Actual)*

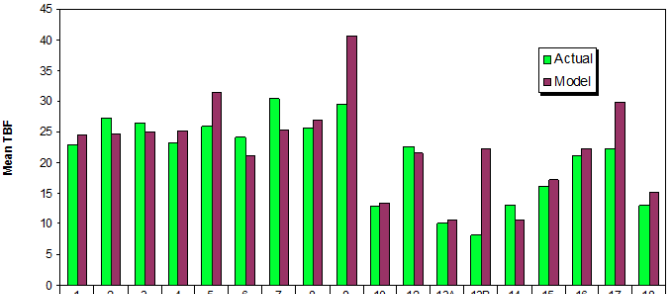

	1	2	3	4	5	6	7	8	9	10	12	13A	13B	14	15	16	17	18
Actual	22.95	27.36	26.46	23.29	25.84	24.09	30.33	25.78	29.56	12.89	22.52	10.16	8.183	13.06	16.15	21.23	22.23	12.99
Model	24.42	24.71	25.05	25.16	31.48	21.22	25.31	27.01	40.74	13.31	21.62	10.58	22.25	10.58	17.19	22.26	29.97	15.04

Fig. 7 *Comparison of Mean TBF (Model vs. Actual)*

Traditional simulation models use the distributions for TTR and TBF that capture the static characteristic, but not the dynamics. In this investigation, nonlinear dynamics characterization methods, for e.g., recurrence quantification analysis, are used to extract quantifiers for deciding the dimension of the state vector and functional forms of vector fields of n-SDE models. Complex dynamics of manufacturing and other real-world systems can be effectively captured using nonlinear stochastic dynamic models of the form:

$$d\underline{x} = \underline{F}(\underline{x})dt + \underline{\underline{g}}(\underline{x})d\underline{\beta} \qquad (10)$$

where $\underline{x}$ is a m-dimensional state vector, $\underline{F}(\bullet)$ is usually a nonlinear vector field, and the stochastic term $\underline{\underline{g}}(\underline{x})\mathrm{d}\underline{\beta}$ accounts for the influence of extraneous phenomena. Nonetheless, in many real life cases, only a few process output measurements y (e.g., throughput variations, WIP levels) or coupled high dimensional measurements are available in lieu of the complete state vector $\underline{x}$. Takens' embedding theorem stated in the following provides a means for state space reconstruction from y.

Takens' delay embedding theorem (1981) [15]**:** *Let* **M** *be a compact manifold of topological dimension d. For pairs* (ϕ, *h*)*, where* ϕ: **M** → **M** *is a smooth* (*at least* C^2) *diffeomorphism and h*: **M** → **R** *a smooth function, it is a generic property that the* (2*d*+1) *- fold observation map* H_k [ϕ, *h*]: **M** → $\mathbf{R}^{2d+1}$ *defined by*

$\underline{x} \mapsto (\mathrm{h}(\underline{x}), \mathrm{h}(\phi(\underline{x})), \ldots, \mathrm{h}(\phi^{2d}(\underline{x})))$ *is an immersion* (*i.e.* H_k *is one-to-one between M and its image with both* H_k *and* H_k^{-1} *differentiable*).

Takens' delay embedding theorem shows the system dynamics can be adequately reconstructed by using the time-delay coordinates of the individual measurements because of the high dynamic coupling existing in physical system. For discrete time series y (see Fig. 8(a) for illustration), state vector $\underline{x}$ (Fig. 8(b)) is reconstructed using a delay sequence of points in $\{y(t_n)\}$ as,

$$\underline{x}(t_n) = [y(t_n),\ y(t_n+\tau),\ y(t_n+2\tau),\ \ldots,\ y(t_n+(m-1)\tau)] \qquad (11)$$

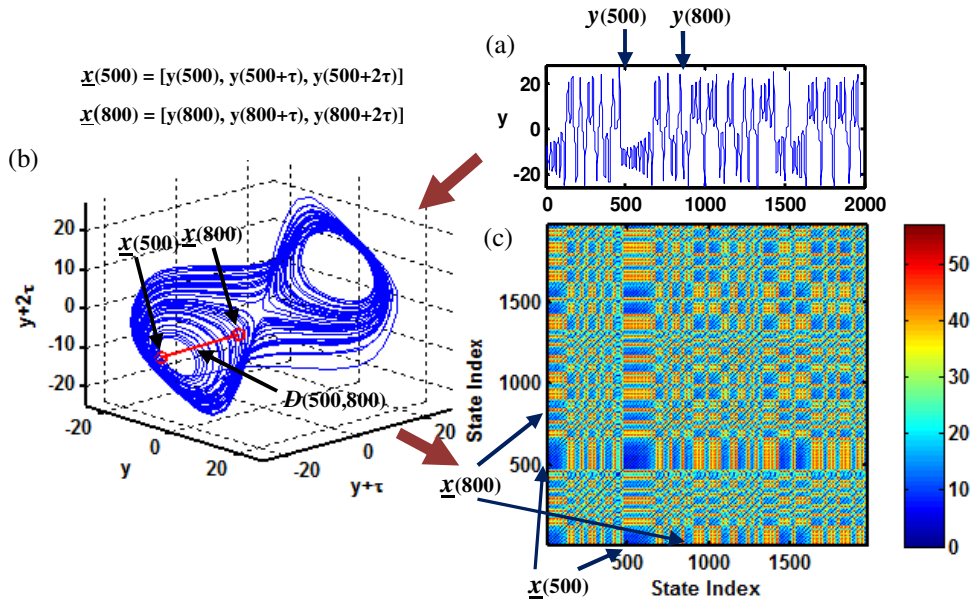

Fig .8 Graphical illustration of the relationship among Lorenz time series, attractor and recurrence plot

where m is the embedding dimension ($m \geq 2d+1$) and τ is the time delay. The optimal sufficient embedding dimension m to unfold the attractor is determined by false nearest neighbor method [16]. Mutual information function [17] is used to minimize both nonlinear dynamic and linear correlations for the choice of optimal time delay τ. System dynamics often manifest in the vicinity of an attractor $\mathbf{A}$ (e.g., Lorenz attractor [18] shown in Fig. 8(b)), which is an invariant set defined in an m-dimensional state space.

System dynamics exhibit recurrence characteristics as stated in the following theorem.

Poincare recurrence theorem (1890) [19]: *Let* T *be a measure-preserving transformation of a probability space* ($\mathbf{A}$, μ), *and let* $\Omega \subset \mathbf{A}$ *be a measurable set. Then for any* $J \in \square$, $\mu(\{\underline{x} \in \Omega | \{T^j(\underline{x})\}_{j \geq J} \subset \mathbf{A} \backslash \Omega\}) = 0$.

Poincare recurrence theorem implies that if one has a measure preserving transformation, the trajectories eventually reappear at neighborhood Ω of former points with probability one. Recurrence plots (see Fig. 8(c)) capture the topological relationships (including several nonlinear dynamics and non-stationarity related manifestations) existing in this state-space as a 2-dimensional representation. It delineates the distances of every point $\underline{x}(t_i)$, the state vector realized at time t_i, to all the others in the reconstructed state space, i.e., $D(t_i, t_j) := \Theta(\|\underline{x}(t_i) - \underline{x}(t_j)\|)$, where $\|\cdot\|$ is a distance measurement (e.g., the Euclidean norm) and $\Theta(\cdot)$ is the color code that maps the distance to a color scale [20]. As shown in Fig. 8, the distances between the 500th and 800th points in the state space is shown as a color code at the coordinates (500,800) and (800, 500) of the recurrence plot. If the color code at the recurrence plot is blue, then the points are located close to each other in the state space, and if the color code is red, the points are located farther apart. The separations between dark diagonal lines (along 45° degree) indicate the time periods between the recurring system behaviors over certain time segments. Recurrence-based methods have of late shown potential for representation and de-noising of measurements from complex systems [21, 22].

Fig. 9 shows representative unthresholded (top) and thresholded (bottom) recurrence plots of TBF and TTR for n-SDE, actual and exponential models from an assembly line segment. Recurrence plots from n-SDE and actual model show complex (nonlinear) and irregular (stochastic) texture patterns while the one from exponential model shows complete noise. The more blue (dark shade) and more yellow shade indicate the underlying nonstationarities in the signal.

Clearly, n-SDE model captures the certain intriguing and visually appealing patterns underlying the measured throughput data. The color map captures recurrence points identified at different neighborhood sizes. It may be noted that the patterns along vertical segments between two consecutive marked time indices are similar and nearly shifted versions of each other. Thus it is evident that recurrence patterns from the n-SDE model more closely capture the dynamics from actual data compared to a conventional exponential distribution model. The following recurrence quantifiers were used as metrics to quantify these recurrence patterns: (1) Recurrence rate, which measures the density of points in the recurrence plots; (2) Determinism, which measures the predictability of the system and is expressed in terms of the number of lines in the recurrence plot which lengths exceeding a specified threshold of l_{min}; (3) Laminarity that captures the mixing rates of the system; (4)

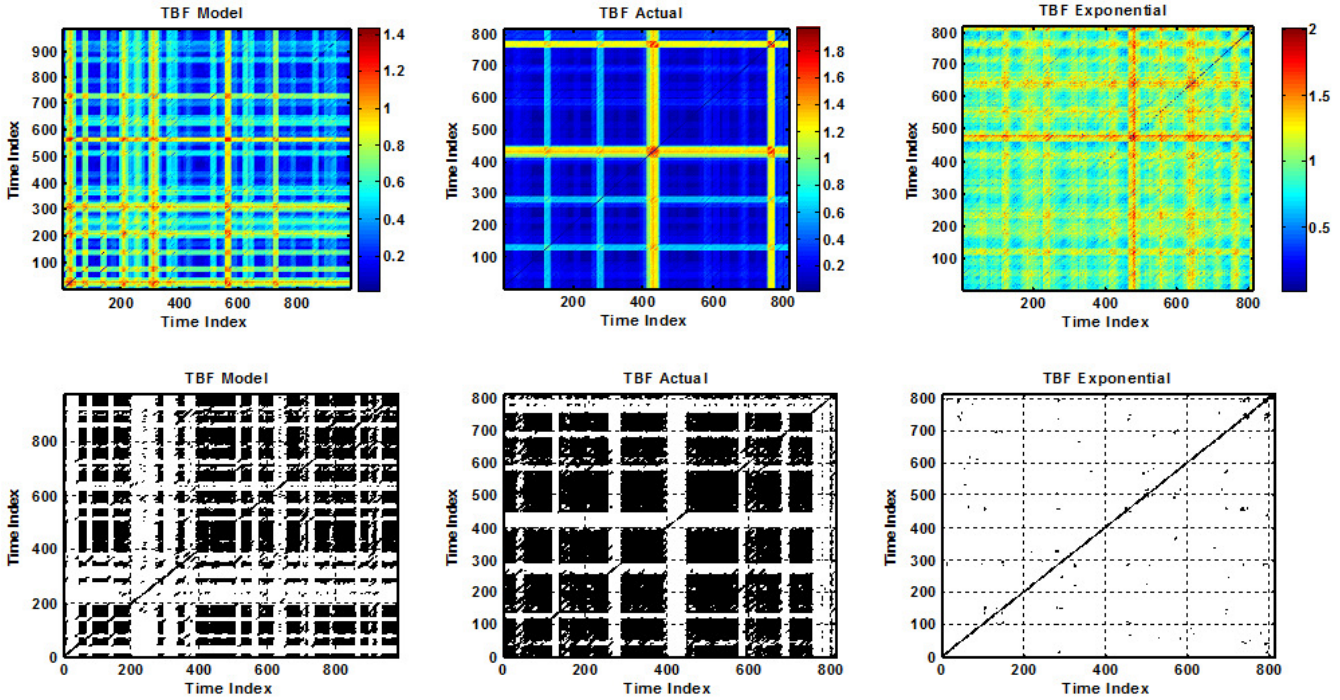

Fig. 9 Comparison of TBF Recurrence Plots for Model, Actual and Exponential

Trapping time, which provides a measure of how long the system remains in a specific state; (5) Linemax which quantifies the divergence rates of trajectories in the system; (6) Shannon entropy that captures the complexity of the deterministic structure; and (7) Trend that determines the rate at which the density of the recurrence plots fade from the diagonal line.

Table 4 and Table 5 compare the quantifiers (quantification of recurrence plots) for TTR and TBF. As stated in the foregoing, these metrics are based on the recurrence point density, diagonal lines, and vertical lines structures of the recurrence plots [20, 23]. It may be noted that the exponential model recurrence rate is much smaller than that of n-SDE model and actual data in Table 4 and Table 5. This means that TBF and TTR data from exponential model are seldom recurrent, and the patterns tend to be more random. Correlations from the actual operations are not tracked and captured. While the n-SDE model recurrence rate is much closer to that of actual data. It is more likely to capture the underlying recurrence dynamics of actual operations.

TABLE 4. COMPARISON OF TBF RECURRENCE QUANTIFIERS FOR MODEL, ACTUAL AND EXPONENTIAL

Metric	TBF			TBF Error %	
	Actual	Model	Exp	Model	Exp
Recrate	39.94	24.70	0.04	38%	100%
Determinism	97.48	96.94	25.32	1%	74%
Laminarity	115.00	82.00	8.00	29%	90%
Entropy	5.55	4.89	1.84	12%	62%
Trend	0.04	0.02	0.01	50%	50%
Linemax	90.70	91.25	0.00	-1%	100%
Trap. time	30.72	25.73	NaN	16%	>>100%

TABLE 5. COMPARISON OF TTR RECURRENCE QUANTIFIERS FOR MODEL, ACTUAL AND EXPONENTIAL

Metric	TTR			TTR Error %	
	Actual	Model	Exp	Model	Exp
Recrate	43.24	21.78	0.13	50%	99%
Determinism	97.84	97.90	51.31	0%	48%
Laminarity	115.00	102.00	30.00	11%	71%
Entropy	5.71	4.65	2.38	19%	49%
Trend	0.04	0.04	0.01	0%	75%
Linemax	92.08	95.32	0.00	-4%	100%
Trap. time	33.01	29.10	NaN	12%	>>100%

Table 4 and Table 5 reveals that most of the recurrence quantifiers from n-SDE model are much closer to actual compared to those from an exponential model. These results provide strong evidence that the present n-SDE modeling approach is superior to the commonly used exponential and other parametric distributions to capture TBF and TTR processes. Further investigations are necessary to develop this approach for effective (faster and more accurate) fitting of the downtime distributions and their interrelationships.

IV. CONCLUSIONS

The present work implemented analytical nonlinear stochastic differential equation (n-SDE) models to capture the dynamics of automotive manufacturing systems. Sigmoid function theory has been used to model downtime as the interplay between a machine degradation and restoration efforts. The n-SDE modeling approach was experimented on an 18 station assembly line segment in Matlab's Simulink© environment. The results were compared with those from a real-world production line observed during approximately one-year long period. The results show that n-SDE model is significantly better at capturing the distribution of (marginal probability) of TBF and TTR compared to commonly used exponential distribution models. The model is also able to capture the salient trends in the assembly line dynamics, including the relative throughput losses due to blocking, starving, and machine breakdown. An extensive set of metrics were used to compare the statistical and nonlinear dynamical behaviors gathered from the models versus actual assembly line data. The model was found to capture the recurrence and other nonlinear behaviors of the assembly line dynamics better than conventional exponential distribution based models.

Our ongoing investigations will consider additional nuances of degradation dynamics (e.g., various structures for different modes of failure) and their implications on computational complexity and accuracy of simulations relative to the actual observations. We will also study the use of alternative sigmoid functional forms and the effects of linearization of the model on the stability and computational efficiency.

REFERENCES

[1] K. K. B. Hon, "Performance and Evaluation of Manufacturing Systems," *CIRP Annuals,* vol. 54, p. 675, 2005.

[2] D. Armbruster, G. Radons and R. Neugebauer, *Dynamical Systems and Production Systems, Chapter I in Nonlinear Dynamics of Production Systems*. Berlin: Wiley-VCH, 2004.

[3] D. Armbruster, and C. Ringhofer, "Thermalized kinetic and uid models for re-entrant supply chains," *SIAM J. Multiscale Modeling and Simulation,* In print 2005.

[4] D. Armbruster, R. Chidambaram, G. Godding, K. Kempf, and I. Katzorke, "Modeling and analysis of decision flows in complex supply networks," in *Proceedings of POMS*, Sao Paulo, 2001, pp. 1106 -1114.

[5] D. Armbruster, D. Marthaler, and C. Ringhofer, "Kinetic and fluid model hierarchies for supply chains," *SIAM Multiscale Modeling and Simulation,* vol. 2(1), pp. 43-61, 2004.

[6] D. Armbruster, C. Ringhofer, and T.-J. Jo, "Continuous models for production flow," in *American Control Conference*, Boston, 2004, pp. 4589 - 4594.

[7] D. Armbruster and E. S. Gel, "Bucket brigades revisited: Are they always effective?," *European Journal of Operational Research,* vol. 172, pp. 213-229, 2006.

[8] J. Westman, and F. Hanson, "Computational Method for Nonlinear Stochastic Optimal Control," in *Proceedings of the 1999 American Control Conference*, 1999, pp. 2798-2802.

[9] N. Duffie, and I. Falu, CIRP "Control-theoretic analysis of a closed-loop PPC system," *Annals - Manufacturing Technology,* vol. 51, pp. 379-382, 2002.

[10] H. Wiendahl, and J. Breithaupt, "Backlog-oriented automatic production control," *CIRP Annals - Manufacturing Technology,* vol. 50, pp. 331-334, 2001.

[11] H. Wiendahl, N. Roth, and E. Westkamper, "Logistical positioning in a turbulent environment," *CIRP Annals - Manufacturing Technology,* vol. 51, pp. 383-386, 2003.
[12] H. P. Wiendahl and H. Scheffczyk, "Simulation based analysis of complex production systems with methods of nonlinear dynamics," *CIRP Annals,* vol. 48, p. 357, 1999.
[13] H. Yang, S. T. S. Bukkapatnam, and L. Barajas, "Nonlinear hybrid modeling of assembly line dynamics," *International journal of production research (under review),* 2008.
[14] S. T. S. Bukkapatnam and K. Sadananda, "A genetic algorithm for predictive modeling of fatigue crack growth using unified approach," *International Journal of Fatigue,* vol. 27, pp. 1354-1359, 2005.
[15] Takens, *Detecting strange attractors in turbulence, In Lecture notes in mathematics* vol. 898: Springer, Berlin, 1981.
[16] M. B. Kennel, R. Brown, and H. D. I. Abarbanel, "Determining embedding dimension for phase-space reconstruction using a geometrical construction," *Physical Review A,* vol. 45, p. 3403, 1992.
[17] A. M. Fraser and H. L. Swinney, "Independent coordinates for strange attractors from mutual information," *Physical Review A,* vol. 33, p. 1134, 1986.
[18] E. N. Lorenz, "Atmospheric predictability as revealed by naturally occurring analogues," *Journal of Atmosphere Sciences,* vol. 26, pp. 636-646, 1969.
[19] A. Katok and B. Hasselblatt, *Introduction to the Modern Theory of Dynamical Systems*, 1 ed.: Cambridge University Press, 1995.
[20] J.-P. Eckmann, S. O. Kamphorst, and D. Ruelle, "Recurrence plots of dynamical systems," *Europhys Lett,* vol. 4, pp. 973-977, 1987.
[21] H. Yang, M. Malshe, S. T. S. Bukkapatnam, and R. Komanduri, "Recurrence quantification analysis and principal components in the detection of myocardial infarction from vectorcardiogram signals," in *Proceedings of the 3rd INFORMS Workshop on Data Mining and Health Informatics (DM-HI)*, Washington, DC, 2008.
[22] S. Bukkapatnam, "Compact nonlinear signal representation in machine tool operations," in *ASME Design Engineering and Technology Conference, DETC-VIB 8068*, Las Vegas, NV, September 12-15, 1999.
[23] N. Marwan, M. Carmen Romano, M. Thiel, and J. Kurths, "Recurrence plots for the analysis of complex systems," *Physics Reports,* vol. 438, pp. 237-329, 2007.

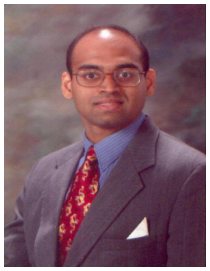

Satish T. S. Bukkapatnam received the Ph.D. degree in industrial and manufacturing engineering from Pennsylvania State University, University Park. He is an Associate Professor with the School of Industrial Engineering and Management, Oklahoma State University. He has previously served as a summer Faculty Consultant at the U.S. Naval Research Laboratory and an Assistant Professor of Industrial and Systems Engineering at the University of Southern California (USC). His research in sensor-based modeling is a fundamentally new approach to improve quality and performance of manufacturing machines and processes, and other real-world complex systems. These systems include structural systems, the Internet, and a variety of infrastructure systems of interest to IT, transportation, medical, and defense enterprises. This approach is based on augmenting the statistical and intelligent systems foundations of modern monitoring technologies with nonlinear dynamics principles.

Dr. Bukkapatnam was a recipient of Alpha Pi Mu/Omega Rho Outstanding Teacher of the Year in Industrial Systems Engineering, USC, in 2002, and the SME Dougherty Outstanding Young Manufacturing Engineer Award.

Hui Yang was born in Nanjing, Jiangsu province, P.R.China. He received his Ph.D. degree from the school of Industrial Engineering and management at Oklahoma State University.

He is a member of IEEE (Institute of Electrical and Electronics Engineers), INFORMS (Institute for Operations Research and Management Science), and IIE (Institute of Industrial Engineers).

Utkarsh Mittal was born in Roorkee, Uttranchal, India. He received his Masters degree from the school of Industrial Engineering and management at Oklahoma State University. He is currently working as a Project Engineer in GE Energy.

Leandro G. Barajas (S'95–M'99–SM'06) was born in Bogotá, Colombia, in 1973. He received the Honor degree in electronics engineering as Valedictorian from the Universidad Distrital F.J.C., Bogotá, Colombia, in 1998, and the M.S. and Ph.D. degrees in electrical and computer engineering from the Georgia Institute of Technology (Georgia Tech), Atlanta, in 2000 and 2003, respectively. He is currently a Senior Research Engineer at the General Motors R&D Center, Manufacturing Systems Research Laboratory,Warren, MI, where he focuses on the area of Plant Floor Systems and Controls. During his graduate studies, he worked at the Center for Board Assembly Research (CBAR), Manufacturing Research Center (MARC), Georgia Tech.

Dr. Barajas is a Senior Member of the Society of Manufacturing Engineers (SME), Elected Full Member of SIGMA XI (The Scientific Research Society), member of the societies Automotive Engineers (SAE), Hispanic Professional Engineers (SHPE), and the Surface Mount Technology Association (SMTA). In 2000 and 2003, he receivedM.S. and Ph.D.OMED Tower Awards from Georgia Tech. During his tenure at GM, he has been distinguished with the 2005 GM R&D "Spark-Plug" Award, the 2006 GM Chairman's Honors Award, the 2006 GM R&D Charles L. McCuen Special Achievement Innovation Award, and the 2007 SME Kuo K. Wang Outstanding Young Manufacturing Engineer Award.